Resonances in ^{14}C observed in the ^{4}He(^{10}Be,α)^{10}Be reaction

M. Freer,[1] J. D. Malcolm,[1] N. L. Achouri,[2] N. I. Ashwood,[1] D. W. Bardayan,[3,*] S. M. Brown,[4] W. N. Catford,[4] K. A. Chipps,[3] J. Cizewski,[5] N. Curtis,[1] K. L. Jones,[6] T. Munoz-Britton,[1] S. D. Pain,[3] N. Soić,[7] C. Wheldon,[1] G. L. Wilson,[4,†] and V. A. Ziman[1]

[1]*School of Physics and Astronomy, University of Birmingham, Edgbaston, Birmingham, B15 2TT, United Kingdom*

[2]*LPC Caen, ENSICAEN, Université de Caen, CNRS/IN2P3, Caen, France*

[3]*Physics Division, Oak Ridge National Laboratory, MS-6354, Building 6010, P.O. Box 2008, Oak Ridge, Tennessee 37831-6354, USA*

[4]*School of Electronics and Physical Sciences, University of Surrey, Guildford, Surrey, GU2 7XH, United Kingdom*

[5]*Department of Physics and Astronomy Rutgers, The State University of New Jersey, 136 Frelinghuysen Road, Piscataway, New Jersey 08854-8019, USA*

[6]*Department of Physics and Astronomy, University of Tennessee, Knoxville, Tennessee 37996, USA*

[7]*Rudjer Bošković Institute, Department of Experimental Physics, Bijenička 54, HR-10000 Zagreb, Croatia*

(Received 7 July 2014; revised manuscript received 17 October 2014; published 19 November 2014)

The α(^{10}Be, α)^{10}Be resonant scattering reaction has been measured at nine ^{10}Be beam energies from 25 to 48 MeV, scanning out resonances in ^{14}C from excitation energies of 13 to 24 MeV. Angular distribution measurements were used to assign the spin and parity of 5^- to resonances at $E_x = 18.82(2)$ and 19.67(2) MeV and 6^+ at $E_x = 20.80(2)$ MeV. The data also strongly indicate a 3^- resonance at 17.32(2) MeV. The systematic uncertainty on the excitation energies is 175 keV. An R-matrix analysis has been performed for the excitation energy range 16.5 to 22 MeV. The data are discussed in terms of cluster bands in ^{14}C.

DOI: 10.1103/PhysRevC.90.054324 PACS number(s): 21.10.−k, 23.20.En, 25.40.Ny, 27.20.+n

I. INTRODUCTION

The understanding of the structure of the nucleus ^{12}C has developed considerably in recent times, as knowledge of the spectroscopy above the α-decay threshold has improved. For example, the 2^+ excitation of the Hoyle state has been discovered close to 10 MeV [1–5] and there is evidence for a 4^+ excitation [6]. The ground state of ^{12}C is associated with an oblate structure with a triangular D_{3h} point symmetry [7]. The Hoyle state, which lies above the α-decay threshold, has a well-developed cluster structure, though the precise nature of the state remains to be fully determined. However, the possibility that the state is associated with a linear 3α configuration has been excluded [3].

The addition of one or more neutrons to these structures could be associated with $3\alpha + Xn$ type configurations, where the symmetries and structure of ^{12}C continue to play a role. The characterization of such nuclei above the α-decay thresholds is thus of interest to determine whether the transition to dominant clustering above the α-decay threshold, observed in ^{12}C, is found. From a theoretical perspective there are strong indications that, for example, in ^{14}C the ^{10}Be + α structure is rather important above the α-decay threshold of 12.01 MeV but less so below the threshold [8].

A comprehensive analysis of states in ^{13}C [9] and ^{14}C [10] provided evidence for a series of oblate and prolate bands. In this instance, the intrinsic 3α structure remained influential and the valence neutrons were exchanged between the cores in a manner which is similar to the exchange of electrons in covalent molecules. These structures have been identified with rotational bands whose bandheads lie below the α-decay threshold. If the structure that is found in ^{12}C is mirrored in ^{13}C and ^{14}C, then the below-threshold symmetries associated with the clusters are present, but the cluster structure itself is suppressed.

From the experimental side, there have been a number of measurements of the α decay of excited states of ^{14}C. For example, such states have been seen in the ^{7}Li(^{9}Be,^{14}C*)^{2}H [11], ^{14}C(^{14}C,^{14}C*) [12], and ^{14}C(^{13}C,^{14}C*) [13] reactions. The present status of α-decaying states is summarized in Ref. [14], which presents measurements using the ^{12}C(^{16}O,^{14}O)^{14}C reaction. The measurements of the ^{12}C(^{6}He,^{4}He)^{14}C reaction also provide insight into cluster-like states in ^{14}C [15]. However, for the most part, the data are limited from a statistical perspective and there are few suggestions for spins and parities. Hence, an understanding of the structure above the threshold has not been reached.

This paper presents an investigation above the α-decay threshold using the ^{10}Be + α resonant scattering reaction in which a high-statistics ^{14}C resonant spectrum is determined and angular distributions of the reaction products are used to indicate possible resonance spins.

II. EXPERIMENTAL DETAILS

The technique of resonance scattering using a thick target was first developed at the Kurchatov Institute [16]. It involves the passage of a beam through a thick target material. As the beam slows down, and the center-of-mass energy coincides with that of a resonance of the projectile-target composite

*Present address: Institute for Structure and Nuclear Astrophysics, Department of Physics, University of Notre Dame, Notre Dame, IN 46556, USA.

†Present address: Department of Physics University of York, Heslington, York, YO10 5DD, United Kingdom.

system, a resonant component to the scattering process occurs. Typically, the target has a lower mass than the projectile, the beam is stopped in the target, and the resonant decay by light particle emission may be observed at 0°. This technique is thus appropriate for the characterization of proton and α decay widths of excited states. In the present case a thick helium-4 gas target was used with a ^{10}Be beam with silicon detectors in the forward direction to pick up the α decay of ^{14}C resonances.

For such an arrangement, resonances are formed at different depths within the gas volume and hence at different distances from the detection system; each resonance corresponds to a particular excitation energy in the composite system. Consequently, the solid angle intercepted by the detection system varies with excitation energy—an effect that can be corrected using Monte Carlo simulations.

Furthermore, the decay of a resonance to excited states in the final-state particles (in the present case ^{10}Be) can contribute. In this instance, due to the loss of some of the final-state kinetic energy to the inelastic excitation, the energy of the detected products is reduced and this can be misinterpreted as a resonance with the incorrect energy. These two features can complicate the analysis, though, as explained later, both have been accounted for.

The measurements were performed using a previously prepared ^{10}Be sample placed in the ion source of the HRIBF tandem accelerator at Oak Ridge National Laboratory (ORNL). Nine beam energies between 25 and 48 MeV were used: 25, 27, 29, 32, 34, 38, 40, 44, and 48 MeV. The ^{10}Be beam had an intensity of 10^6 particles/s. The beam purity was $>$99%, which was achieved through the use of a secondary stripper foil (80 μg cm^{-2} carbon) in advance of the HRIBF tandem analyzing magnet to fully strip both the ^{10}Be beam and the ^{10}B contaminant. This resulted in most of the ^{10}B being removed from the beam.

The helium-4 gas was maintained at a pressure of 830 mbar and was contained within the reaction chamber using a 5-μm-thick Havar window. This pressure was close to the calculated maximum that the Havar window could sustain. In passing through the window the beam lost between 4.9 and 3.2 MeV, for beam energies of 25 and 48 MeV, respectively. The estimated uncertainty in the thickness of the window is 10%, which in turn gives an uncertainty in the beam energy on entry into the chamber of 320 keV at 48 MeV and 520 keV at 25 MeV.

The beam then slowed through the gas volume along an interaction path of 38 cm, tracing out an excitation function. The α particles produced from either elastic scattering or the resonant decay of ^{14}C were then detected at forward angles [backward angles in the center-of-mass (c.m.) frame] and, in particular, in the telescope at 0° (180° in the c.m. frame). The energy loss of the α particles in the gas for events near the window at 25-MeV beam energy was 2.2 MeV (with an uncertainty of 2% in the gas pressure, 16 mbar, giving an uncertainty of 40 keV on this α-particle energy). At 48-MeV energy the energy loss was 1.04 MeV and hence uncertainty from that in the gas pressure would be 20 keV. This uncertainty in the energy loss in the gas is larger than the uncertainty in the path length, which is estimated to be 1%.

The ^{10}Be beam was eventually stopped, after 38 cm, in Mylar foil of thicknesses of 46 and 144 μm (the latter thickness being used for beam energies $\geqslant$38 MeV). The energy loss of the α particles in the Mylar absorber for the 25-MeV beam was 2.6 MeV. Consequently, a 10% uncertainty in the foil thickness would translate into a 260-keV uncertainty in the detected α-particle energy. At 48 MeV, with the thicker absorber the energy correction to the α-particle energies is up to 4.6 MeV for reactions taking place close to the 0° detectors (Mylar stopper). A 10% variation would give a 460-keV shift in the α-particle energy. It should be noted that the agreement with the excitation energy spectra above $E_{\rm beam} = 38$ MeV and below this energy (when the foil thickness was changed) indicates that the corrections have been performed correctly and uncertainties in the thickness of the Mylar absorbers do not dominate. Nevertheless, the maximum theoretical uncertainties in the α-particle energies from those in the gas pressure and the thickness of the Mylar stopping foils are 265 and 461 keV for beam energies of 25 and 48 MeV, respectively. Translated into uncertainties in ^{14}C excitation energies, this corresponds to 76 and 132 keV.

The uncertainty in the beam energy as it enters the region containing the helium-4 gas has, in comparison, a negligible effect on the energy of the α particles, fractionally changing the energy losses of the beam and emitted α particles in the gas. However, this uncertainty instead alters the location of where the interaction takes place within the chamber, along the 38-cm-long path. In turn, this creates uncertainty in the reconstruction of the emission angles, which is important for the measurements of the angular distributions (see later). Typically, the uncertainties quoted above for the beam energy would translate into a distance of 1.5 to 2 cm, to be compared with the 38-cm path length.

Directly behind the Mylar foils were three 1-cm-diameter silicon detectors of thicknesses of 100, 150, and 200 μm. These formed a ΔE_1-ΔE_2-E particle identification telescope. The telescope was capable of identifying the α particles produced in the resonant scattering reaction. In fact, only α particles and lighter particles were observed to be transmitted by the Mylar foils.

Away from the beam axis, 0°, there were two arrays of large silicon detectors. These were YY1 wedge-shaped detectors [17], which were 500 μm thick. The construction of these detectors is such that eight detectors form a 360° disk around the beam axis. In the present case six detectors were formed into a lamp-shade-type configuration [18]. Two such lamp-shade arrays, Lamp1 and Lamp2, were arranged within the gas at 15.5 and 43.9 cm from the window. The inclination of these detectors from the beam axis was 46°. The detectors intercepted angles, measured with respect to the window, of 13.0° to 43.3° and 5.0° to 13.5°, respectively. The experimental arrangement is shown schematically in Fig. 1.

All the silicon detectors were energy calibrated using ^{241}Am and ^{244}Cm α sources. The energy calibration was confirmed for the telescope at higher energies using the energies at which protons, deuterons, tritons, and α particles, produced in reactions with the beryllium beam, punched through the silicon detectors (i.e., ceased to deposit their full energy). The

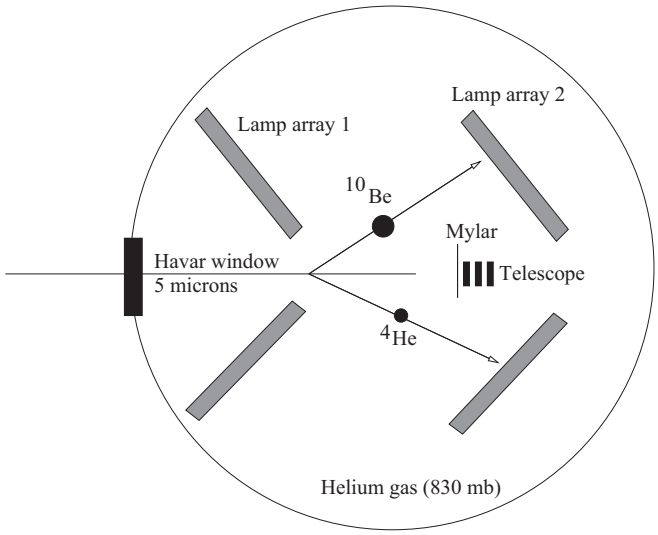

FIG. 1. Experimental arrangement used in the measurements.

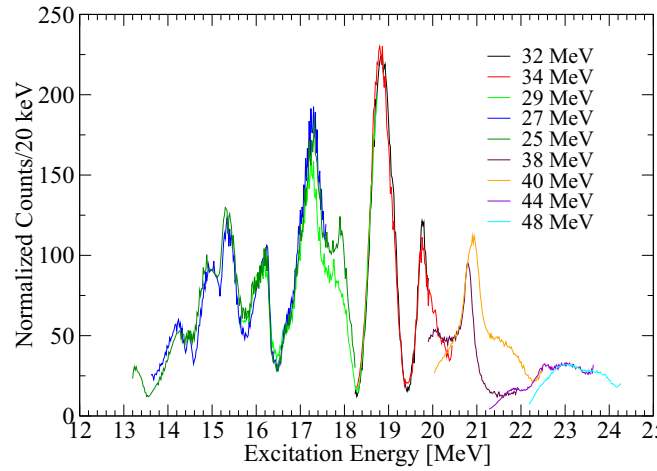

FIG. 2. (Color online) Resonant scattering yields for the nine different beam energies, following the correction for detection efficiency and normalization.

precision with which it was possible to reconstruct the energy of the α particles in the telescope, due to uncertainties in the calibration, was ∼400 keV. Consequently, it is estimated that the overall uncertainty for the excitation energy, including the effects described earlier, was 135 keV (25 MeV) to 175 keV (48 MeV).

The energy calibration of the lamps-hade detectors at energies beyond those of the α-particle calibration source is less reliable as no particle identification and hence punch-through data were available. Consequently, the uncertainties in the energy calibration could be a large as 600–700 keV close to 20 MeV. However, the lamp-shade detectors were used primarily for the angular distribution measurements and hence precise energy calibration was not crucial.

III. EVENT RECONSTRUCTION

The present analysis concerns the detection of α particles from the resonant elastic scattering reaction. In order to determine the center-of-mass energy of the original ^{10}Be + ^{4}He system, the energy of the α particle emitted in the reaction must be determined. This involves correcting the measured α-particle energy first for the energy lost in the Mylar foils and then for the energy lost in the gas between the interaction point and the Mylar foil. The distance traveled by the α particle thus depends explicitly on the energy of the ^{10}Be beam particle at the interaction point. In order to link the energy of the α particle and the center-of-mass energy, a simulation of the energy loss processes, combined with the reaction kinematics, was performed. This was repeated for each beam energy and thickness of the Mylar foils.

Furthermore, for a given resonance in the intermediate system, ^{14}C, with different beam energies, the resonance will occur at a different position along the path through the gas. Correspondingly, the solid angle intercepted by the detectors will thus depend on the beam energy. Consequently, the same simulations which were used to calculate the energy loss dependence, were also used to determine the variation of solid angle. These simulations were then used to normalize the excitation energy spectra.

The resulting excitation functions are shown in Fig. 2 for the nine different beam energies. In the present measurements there was no overall reliable normalization for the beam exposure. Hence, the spectra have been cross normalized, and then the overall normalization was achieved by matching to the Rutherford scattering cross section at the lowest point (see the R-matrix calculations in Sec. V). The common normalization points used, where the data overlap, were close to $E_x = 17.0$, 18.5, 20.2, and 22.8 MeV. The calculated excitation energy spectra coincide well in energy and amplitude. In terms of the excitation energy scale there was agreement between the spectra within 30 keV. The overall systematic uncertainty on the excitation energies is less than 175 keV.

The agreement between the spectra is excellent at lower energies. This would indicate that the contribution from

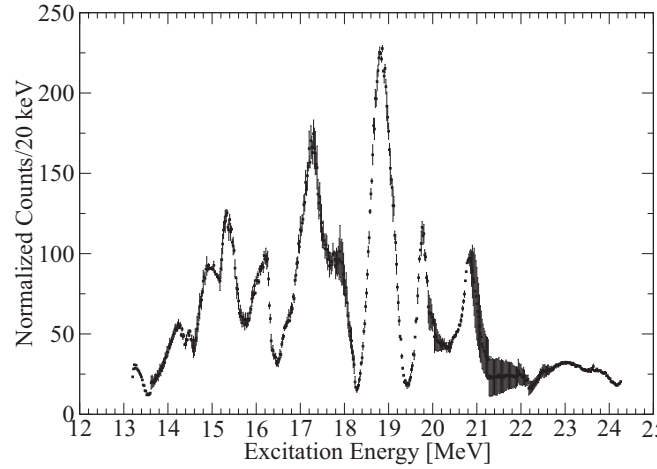

FIG. 3. Excitation function averaged over all of the beam energies. The error bars reflect the standard deviations between the measurements that overlap in excitation energy.

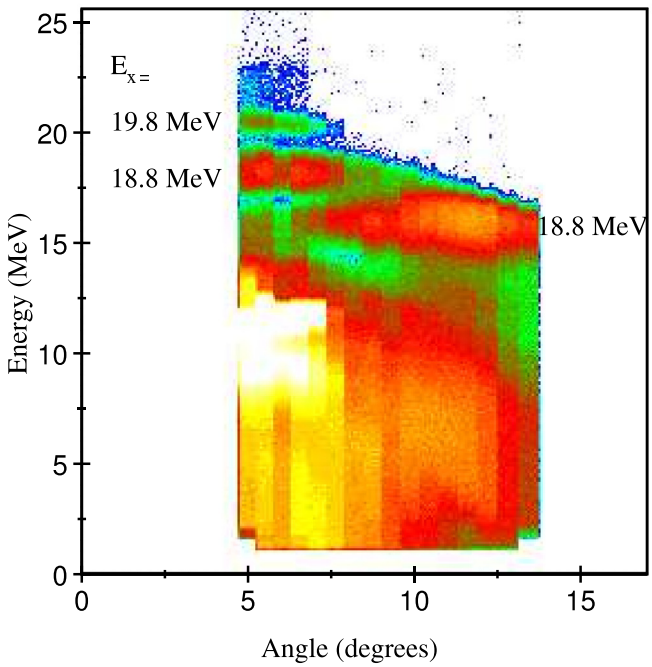

FIG. 4. (Color online) Energy and angle of events in the second Lamp2 detector array for 32-MeV beam energy. The resonances at the excitation energies of 18.8 and 19.8 MeV are indicated for the case when the α particles are detected.

inelastic processes, where the ^{10}Be 3.37-MeV state is excited, is small. There is a discrepancy close to 17.9 MeV, though this cannot be explained by inelastic processes as there are no strong peaks 3.37 MeV higher in energy, which could lead to inelastic contributions. There is also a significant difference found close to 21–22 MeV. This is close to the point where the third detector in the telescope plays a role in the detection. The detector energy threshold compromises the spectra in this region, resulting in a decrease of the experimental acceptance for particular energies. Overall, there is little or no evidence for inelastic processes. An analysis of ^{10}Be + α coincident events was made to attempt to confirm the inelastic contribution, but the data, unfortunately, did not extend into the $\theta_{\text{c.m.}} = 180^\circ$ region.

The nine spectra have been combined by averaging, and the result is shown in Fig. 3, where the error bars correspond to the standard deviation of the overlapping data sets (the statistical errors being significantly smaller). The excitation energy resolution is estimated to be 50 keV. The narrowest structure in the spectra is close to $E_x = 14.5$ MeV in the 27-MeV data and has a width of 90 keV. Hence, there is little evidence that the resolution limits the interpretation of the features in the spectra.

IV. ANGULAR DISTRIBUTIONS

The two lamp-shade detector arrays were used to measure the angular dependence of the yield associated with the resonances observed in Fig. 3. The present analysis is based entirely on the data from the array at the largest distance from the window, which covered the full range of resonance energies. The array closer to the window proved not to provide useful data in this regard.

An example spectrum for the beam energy of 32 MeV is shown in Fig. 4. From Fig. 2, it can be seen that the highest energy locus in Fig. 4 corresponds to the peak close to $E_x =$ 19.8 MeV. This resonance occurs close to the entrance of the chamber and hence the angular range in the downstream lamp-shade array is restricted by the printed circuit boards (PCBs) of the detectors of the upstream lamp-shade array and hence extends only to 7.5°.

At lower energy, between 15 and 20 MeV, is the locus which corresponds to the resonance close to $E_x = 18.8$ MeV.

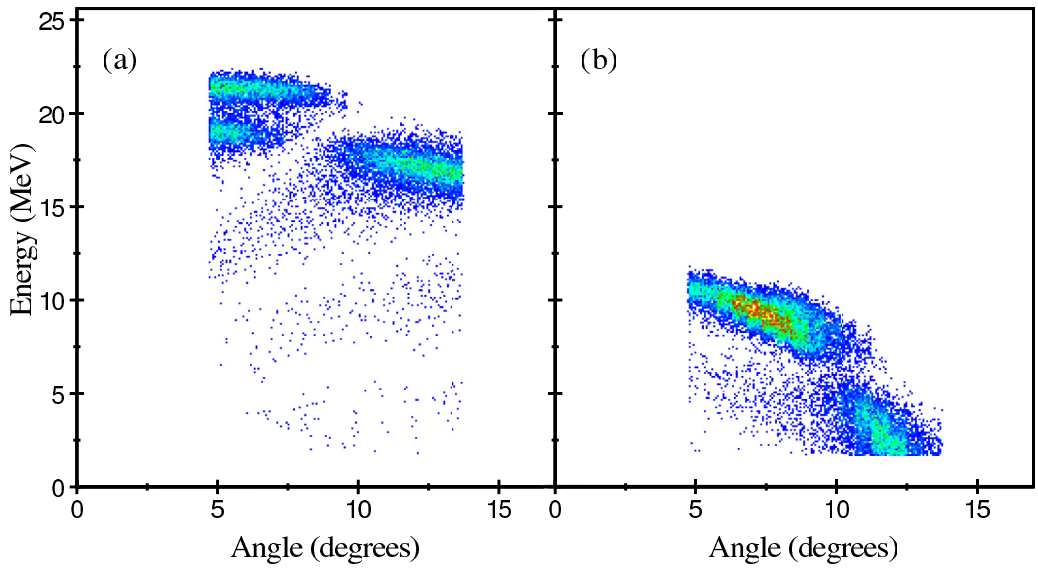

FIG. 5. (Color online) Energy and angle of simulated events in the second Lamp detector array for 32-MeV beam energy for the 18.8- and 19.8-MeV resonances, with $J^\pi = 5^-$, showing (a) the locus for ^{4}He nuclei and (b) that for ^{10}Be nuclei.

In this instance the full range of the distribution is observed, indicating that it occurs beyond the first Lamp array. The intensity as a function of angle is modulated by the discontinuity associated with the azimuthal strips. Also, missing strips in the array cause drops in intensity, as seen for example for the third strip. The intensity as a function of angle is shown in Fig. 6 for the two beam energies of 32 and 34 MeV and for the 18.8-MeV peak. Here the resonance occurs at different points in the chamber and hence the center-of-mass angular range will be different for the two cases. For these one-dimensional angular distributions, Figs. 6 to 10, the effect of the missing strips has been corrected for.

In order to determine the spin of the $E_x = 18.8$ MeV resonance, the angular distributions have been compared with Legendre polynomials. However, this comparison should be made within the center-of-mass frame. The transformation into this frame is challenging as it requires knowledge of where the interaction takes place within the gas, along the path of the beam. Consequently, in order to compare the theoretical distributions with the experimental data a series of simulations have been performed for a variety of spins. These simulations

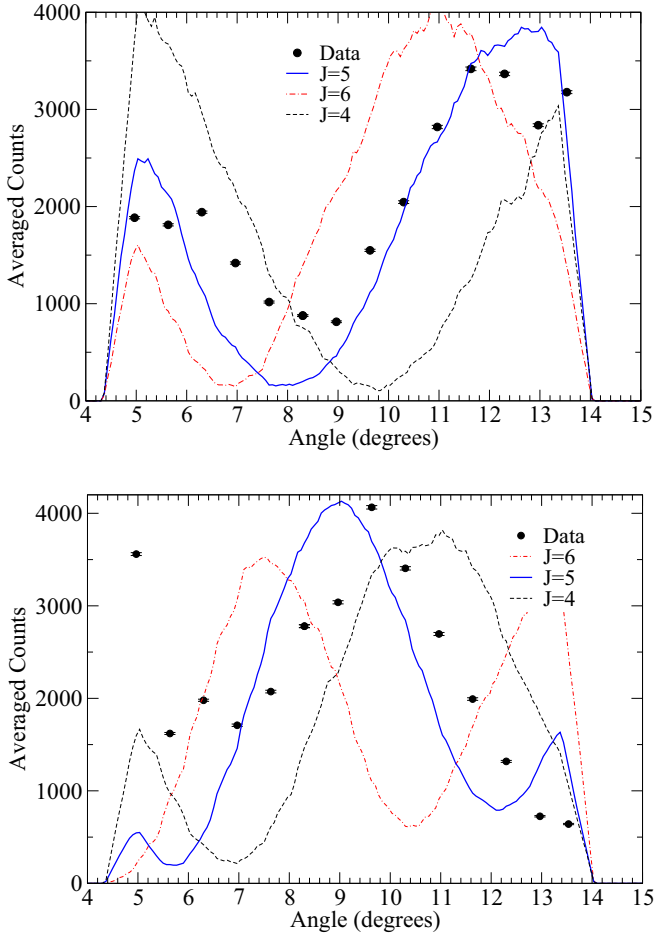

FIG. 6. (Color online) Angular distributions for the peak at $E_x = 18.8$ MeV for beam energies of 32 MeV (top) and 34 MeV (bottom). The experimental data (filled circles) are compared with simulated angular distributions for spins 4, 5, and 6. The experimental data are consistent with a spin of 5.

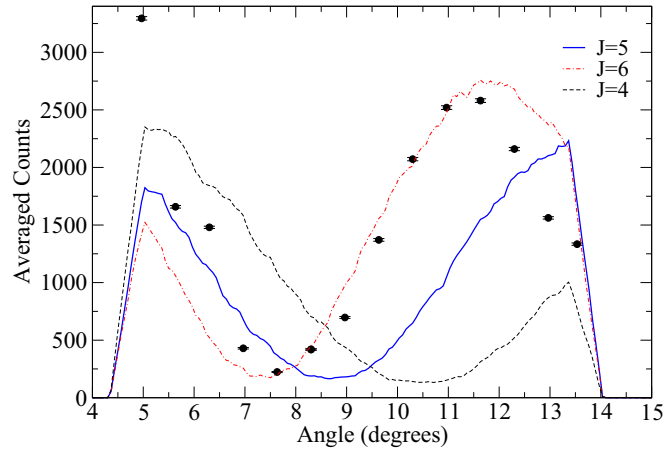

FIG. 7. (Color online) Angular distributions for the peak at $E_x = 20.9$ MeV for a beam energy of 40 MeV. The experimental data (filled circles) are compared with simulated angular distributions for spins 4, 5, and 6. The experimental data are consistent with a spin of 6.

model both the reaction and the energy loss of the beam and reaction products through the gas, based on energy-loss calculations. An example of the simulations for the 18.8- and 19.8-MeV peaks is shown in Fig. 5. It is clear that the two loci at the top of Fig. 4 are linked to the two resonances. The ^{10}Be nuclei are associated with lower energy loci. Figure 4 also indicates scattering of the beam from the Havar window into the Lamp detectors [the high-intensity region at small angles close to 10 MeV (Fig. 4)].

Monte Carlo simulations indicate that the uncertainty in the beam energy due to the precise thickness of the Havar being only known to 10% could lead to shifts in maxima and minima in the angular distributions by up to 3° in the center-of-mass frame. For a spin of 5 (as shown in Fig. 5) the oscillations have an angular frequency of close to 30° and hence in this case the uncertainty in position within the chamber could lead to a 10%

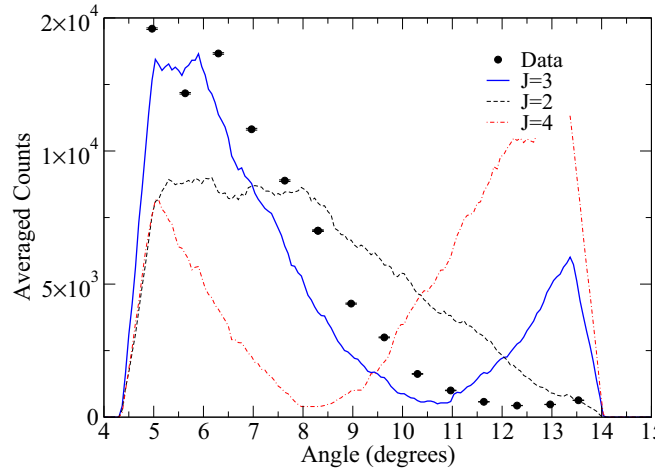

FIG. 8. (Color online) Angular distributions for the peak at $E_x = 17.2$ MeV for a beam energy of 29 MeV. The experimental data (filled circles) are compared with simulated angular distributions for spins 2, 3, and 4. The data are most consistent with a spin of 3.

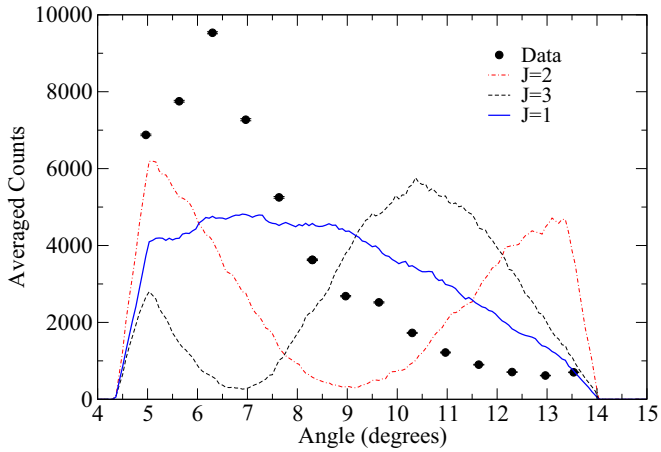

FIG. 9. (Color online) Angular distributions for the peak at $E_x = 16.2$ MeV for a beam energy of 29 MeV. The experimental data (filled circles) are compared with simulated angular distributions for spins 1, 2, and 3. The data are most closely consistent with a spin of 1, though clearly other contributions are included.

shift in the oscillation pattern. Although this is important for matching up precisely the oscillatory features in the angular distributions, it does not preclude the extraction of the spins, which is strongly determined by the oscillation frequency.

The structure as a function of angle shown in Fig. 5 is in good agreement with the experimental data, indicating that the resonance possesses $J^\pi = 5^-$. This is confirmed in Fig. 6, where the data are compared with the simulations for spins 4, 5, and 6. The data are reasonably well reproduced by the $J = 5$ case for the two beam energies of 32 and 34 MeV. The phase is a little different for the 34-MeV data, which reflects the uncertainties in the simulations of energy-loss calculations for the Havar window determining the precise location of the resonance along the interaction path and hence the angle. The shift observed is commensurate with the calculations presented above. Nevertheless, the 5^- assignment is clear.

A similar analysis has been performed across the excitation spectrum range, and the corresponding angular distributions are shown in Figs. 7–10.

The structure in the angular distributions is clearer at higher energies and can be reproduced by single Legendre polynomials. At lower energies the deviation from the Legendre polynomials is significant and indicates a number of contributing angular momenta. In the present analysis we have attempted to identify the dominant component. For example, the data at $E_x = 20.9$ MeV is well reproduced by $J^\pi = 6^+$ (Fig. 7), whereas the distributions at $E_x = 16.2$ MeV indicate low spin (Fig. 9; possibly 1^-); here the reproduction is less convincing. The data for $E_x = 17.2$ MeV (Fig. 8) indicate a dominant $J^\pi = 3^-$ contribution. It should be noted that, due to the presence of $J^\pi = 0^+$ nuclei in both the entrance and exit channels, only natural parity states may be observed: $\pi = (-1)^J$.

V. *R*-MATRIX ANALYSIS

Within the excitation energy region below 16.5 MeV there are a number of resonances for which it is not possible to unambiguously identify their spins, and hence performing an R-matrix analysis is problematic. However, above this energy the angular distributions give a reasonably complete indication of the properties of the resonances. Consequently, an R-matrix analysis has only been performed for the region $E_x = 16.5$ to 22 MeV.

Figure 11 shows an R-matrix fit to the states observed in the spectrum using a 3^- resonance at 17.2 MeV, 5^- resonances at 18.8 and 19.8 MeV, and a 6^+ resonance at 20.9 MeV. In addition, resonances were introduced below this window with 1^-, 2^+, and 4^+ character, as guided by the experimental observations associated with the angular distributions. Furthermore, a 2^+ resonance was introduced

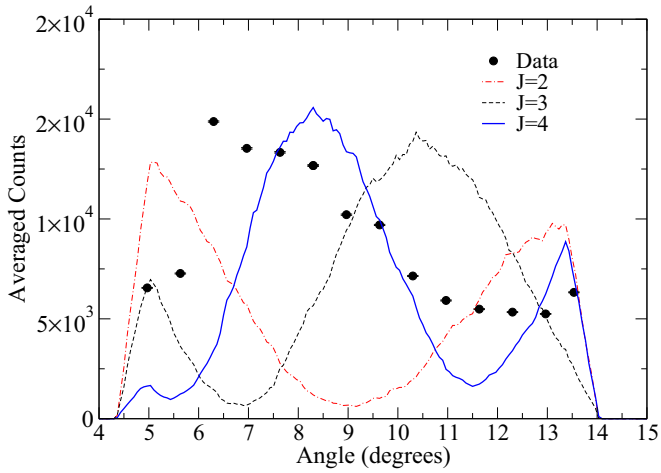

FIG. 10. (Color online) Angular distributions for the peak at $E_x = 15.4$ MeV for a beam energy of 29 MeV. The experimental data (filled circles) are compared with simulated angular distributions for spins 2, 3, and 4. The data are most closely consistent with a spin of 4, as indicated by the peak close to 7°.

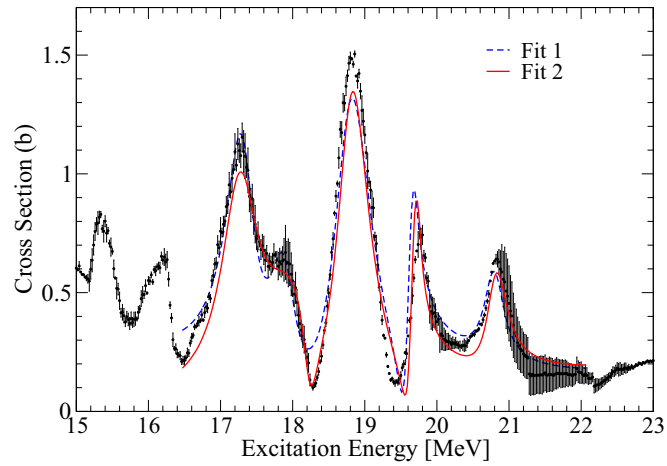

FIG. 11. (Color online) R-matrix fit to the data in the region between $E_x = 16.5$ and 22 MeV (red-solid and blue-dashed lines). The difference between the two fits is the inclusion of an additional 4^+ state in the calculation shown by the red line. See Table I for the parameters of fits 1 and 2.

TABLE I. R-matrix fit parameters for Fig. 11. Fit 1 corresponds to the blue-dashed line and fit 2 to the red-solid line.

Fit 1				Fit 2			
E_x (MeV)	J^π	Γ (keV)	γ (MeV$^{1/2}$)	E_x (MeV)	J^π	Γ (keV)	γ (MeV$^{1/2}$)
17.33	3^-	450	0.36	17.30	3^-	590	0.42
17.95	2^+	420	0.27	17.99	2^+	760	0.36
				18.22	4^+	200	0.27
18.82	5^-	590	0.68	18.83	5^-	500	0.61
19.65	5−	140	0.25	19.69	5^-	100	0.21
20.80	6^+	300	0.48	20.80	6^+	300	0.48

close to 17.8 MeV. This spin and parity were found to offer the best reproduction of the spectrum: $1^-, 2^+, 3^-, 4^+$, and 5^- were all explored. The R-matrix calculations were performed using the AZURE code [19] with a channel radius of 5.2 fm. The fit to the data is indicated by the blue-dashed line shown in Fig. 11, which has been folded with the experimental resolution.

The strong resonance at 18.8 MeV demonstrates interference with neighboring resonances, as indicated by the strong minima in the data at 18.2 and 19.4 MeV. On the high-energy side of the peak this is caused by interference with a higher energy 5^- state. The reproduction of this minimum is not perfect and arises as the fit cannot simultaneously reproduce both the strength and width of the 19.4-MeV 5^- peak. This would suggest a significant neutron-decay branch for this state; an inclusion of such a branch does indeed reproduce the data. On the low-energy side of the 18.8-MeV peak, the reproduction of the minimum is not good. This is improved if a 4^+ resonance is introduced in this region, as indicated by the red line in Fig. 11, which would indicate the presence of a 4^+ state not explicitly observed in the excitation function.

The parameters from the R-matrix analysis are presented in Table I.

VI. DISCUSSION

There are a number of resonances above the α-decay threshold that are tabulated in ^{14}C; Table VII of Ref. [14] provides an up-to-date summary. These have been seen in the ^{7}Li(^{9}Be,^{14}C*)^{2}H [11], ^{14}C(^{14}C,^{14}C*) [12], and ^{14}C(^{13}C,^{14}C*) [13] reactions. In all cases the decay of ^{14}C to $^{10}\mathrm{Be}_{gs} + \alpha$ was observed, and in some instances decays were also measured to excited states of ^{10}Be.

The states which were tabulated as α-decaying in Ref. [14] from the ^{12}C(^{16}O,^{14}O)^{14}C reaction are compared with the present measurements in Table II. At lower excitation energies, $E_x < 17$ MeV, the present data do not substantially constrain the spectrum of states due to the limited information obtainable from the angular distributions. The data appear to indicate contributions associated with $L = 4$ at 15.4 MeV and $L = 1$ at 16.2 MeV. However, these observations cannot be used to make unambiguous assignments of spins of states in this region due to the complexity of the excitation energy spectra.

Since the resonances appear not just as peaks, but can be manifest in terms of both constructive and destructive interference with other resonances and the nonresonant elastic scattering, extraction of resonance parameters requires an R-matrix analysis. However, without a detailed understanding of the nature of the spins, it is not possible to perform such an analysis unambiguously. Nevertheless, many of the features of the excitation energy spectrum in the present measurements are consistent with previously tabulated α-decaying states in this region. For example, at 14.38 MeV in the present measurements there is a dip in the excitation function which coincides with the previously observed 14.3(1)-MeV peak. Similarly, the shape of the spectrum close to 14.75 MeV indicates a feature caused by resonant interference that could correlate with the 14.8(1)-MeV state, etc. It should be noted that a peak in the spectrum, particularly at low energies where the interference with the Rutherford scattering cross section is significant, does not always signify a resonance. We reiterate that consequently it is not possible to arrive at definitive conclusions in this region without spin determinations and R-matrix analysis and that the present data are not inconsistent with other previous measurements in this region.

TABLE II. States tabulated in Ref. [14] as α-decaying states in ^{14}C, together with the present measurements. Items in italics indicate tentative spin-parity assignments or excitation energies (as indicated in Ref. [14]). Bold indicates states that have been reported in more than one reaction. The uncertainties resulting from the R-matrix calculations are shown in brackets and exclude any systematic uncertainty, which could be as large as 175 keV.

E_x	E_x	J^π
14.3(1)	Present measurements	
14.8(1)	possess features	
15.55(10)[a]	consistent with	
15.9	these states	
16.43(10)		
17.3(1)	17.32(0.02)	3^-
18.1	17.97(0.02)	2^+
	18.22(0.02)	4^+
18.5(1), **18.6(1)**	18.82(0.02)	5^-
19.07(1)		
19.3(1)		
19.83(1)	19.67(0.02)	5^-
20.3(1)		
20.6(1)	20.80(0.02)	6^+
21.43(1)		
22.45(3)		
23.15(1)		
24.0(3)		

[a]Assigned $J^\pi = 3^-$ in Ref. [12].

The present analysis offers a rather more unambiguous characterization of the spectrum above 17 MeV. Here, there appears to be a good correlation between the previously reported resonances and those found in the present R-matrix analysis. The previously reported 19.83-MeV state [11–13] coincides with the 19.67-MeV resonance, and the 20.6-MeV state [11,12] is close in energy to the 20.80-MeV resonance reported here. The spins and parities of these resonances were previously undetermined.

In the earlier studies close to the 18.82-MeV state, there are two recorded states at 18.5 MeV [11,13] and 18.6 MeV [12].

These may be the same state. The association with the 18.82-MeV resonance, reported here, is a little uncertain. However, given the uncertainties in the measurement techniques used in Refs. [11–13], and the fact that interference effects were not taken into account in the previous studies, then it is possible that the previously observed states are in fact associated with the present 18.82-MeV state. At the same excitation energy, the analysis presented in Ref. [14] suggested from the measured decay properties that the strength at 18.5 and 18.6 MeV has negative parity with $J = 2$, 4, or 6. States with such unnatural parity would not be observed in the present $^{10}\mathrm{Be} + \alpha$ reaction, which selects only natural parity. In Ref. [14] the α decay was found to proceed to the ^{10}Be 2^+ state, which is consistent with their unnatural parity assignment.

It is highly probable that there are a number of states in this region, with both natural and unnatural parity, and the different reactions and decay paths differentially emphasize the states of varying character.

Of the states measured in the $^{12}\mathrm{C}(^{16}\mathrm{O},^{14}\mathrm{O})^{14}\mathrm{C}$ reaction [14], only the 14.87-MeV state was found to have a measurable width to the $^{10}\mathrm{Be}_{gs} + \alpha$ channel, with the 18.6- and 21.4-MeV states decaying to excited states in ^{10}Be. The 14.87-MeV state has been assigned $J^\pi = 5^-$ (see Refs. [10,14] for further details). Given the proximity to the barrier, a state with this spin would be strongly hindered in terms of α decay [20].

The calculations of the penetrabilities for the neutron and α decay to the ground state indicate that the α decay would be suppressed by a factor of ∼300 [14]. The fact that the α decay is observed points either to the very strong degree of clustering in this state or to the previous spin assignment being incorrect. For example, it is possible that the state observed in the α decay is not the 14.87-MeV 5^- state seen in other reactions, but rather a lower spin state with a similar energy. Similarly, a 6^+ state is known to exist at 14.67 MeV, the contribution of which to the present spectrum would be even more suppressed than that of the 14.87-MeV state.

In summary, the present data provide conclusive spin determinations for a number of ^{14}C states, though it has not been possible to reach firm conclusions for the states at lower energy where the angular distribution measurements are not unambiguous. However, the present data provide the strongest characterization to date.

To understand better the structure of the states, it is possible to compare with the theoretical limit for the α-decay width. The Wigner limit for α decay calculated by using the same channel radius (5.1 fm) as used for the R-matrix calculations is $\gamma = 0.88$ MeV$^{1/2}$. It is clear that a number of states shown in Table I potentially have values of γ quite close to this limit, e.g., ∼0.6 MeV$^{1/2}$ for the 18.82-MeV state. Similarly, the values of γ for the 17.32- and 20.80-MeV states indicate an association with cluster-type structures.

VII. CLUSTER BANDS IN ^{14}C

From a theoretical perspective there are a number of different types of cluster configurations that are possible. The 3α structure found in ^{12}C may be mirrored in ^{14}C with two additional valence neutrons. The three α particles may be geometrically arranged either in an oblate triangular structure or in a prolate linear configuration. The oblate structure has been discussed in Ref. [22], where the $K^\pi = 0^+$ and 3^- bands associated with the rotations of the triangular structure are predicted closely below the α-decay threshold. The predictions coincide well with the known 3^-, 4^-, and 5^- states at 9.80, 11.66, and 14.87 MeV [10]. The corresponding positive-parity states associated with the oblate structure are linked to the 0^+, 2^+, 4^+, and 6^+ states at 6.59, 8.32, 10.74, and 16.43 MeV, respectively [10].

The prolate-type structure is considered in Refs. [10,21,23]. This structure has been linked to positive- and negative-parity bands with the following members: 0^+ (9.75 MeV), 2^+ (10.43 MeV), 4^+ (11.73 MeV), 6^+ (14.67 MeV), 1^- (11.40 MeV), 3^- (12.58 MeV), 5^- (15.18 MeV), and 7^- (18.03 MeV).

The two band structures convincingly follow rotational trajectories with the rotational gradients, $\hbar^2/2I$, of ∼290 keV for the oblate band and ∼120 keV for the prolate band. This indicates, as expected, a larger moment of inertia (I) for the prolate structure. It is clear that the present data do not coincide with either of these proposed rotational bands.

The antisymmetrized molecular dynamics – generator coordinate method (AMD-GCM) calculations presented in Ref. [8] indicate that above the α-decay threshold a multitude of configurations exist, giving rise to a complex spectroscopy. This complexity makes matching between the present measurements and the calculations challenging. However, the calculations do reveal that the $^{10}\mathrm{Be} + \alpha$ structure is well developed above the threshold, in good agreement with the present data.

If the present resonances are strongly mutually linked, then it may be possible to extract a moment of inertia. Figure 12 shows the energy spin systematics, where filled symbols

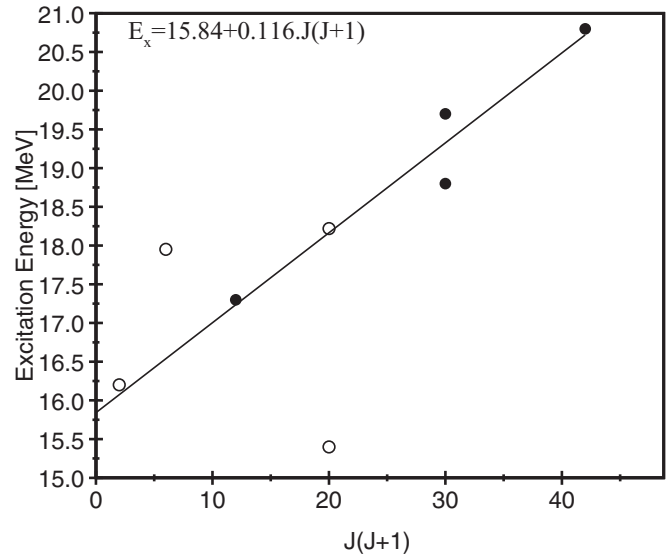

FIG. 12. Energy spin systematics of resonances observed in the present measurements. Solid circles correspond to firm spin assignments, whereas open circles are tentative. The linear fit is to the solid points. The gradient and intercept are 116 keV and 15.84 MeV, respectively.

indicate spins that are more firmly assigned in the present work. A linear fit to these latter set of states indicates a moment of inertia of $\hbar^2/2\mathcal{I} \sim 120$ keV, which is close to that found for the prolate deformed band in Ref. [10]. In order to make further progress, more detailed measurements of the angular distributions at lower excitation energies, $E_x < 17$ MeV, are required. The use of ^{10}Be targets with a ^{4}He beam would be advantageous in this regard.

VIII. CONCLUSIONS

A series of measurements of the $\alpha(^{10}\mathrm{Be},\alpha)$ resonant scattering reaction have been performed which scan a ^{14}C excitation energy range from 13 to 24 MeV, where the α-decay threshold is 12.01 MeV. The measurements provide a high-precision characterization of the excitation energy spectrum and angular distributions which have been used to characterize the spins of many of the resonant states. In particular, we have identified two 5^- resonances at excitation energies of 18.82 and 19.67 MeV, a 6^+ resonance at 20.80 MeV, and a 3^- resonance at 17.32 MeV. An R-matrix analysis indicates that the states have significant α-reduced widths, which would suggest strongly developed $^{10}\mathrm{Be} + \alpha$ cluster structures. It is difficult to place the resonances into rotational bands, but it is possible that they may be linked to highly deformed prolate structures in ^{14}C. To more fully resolve the structural identity more detailed measurements of the angular distributions are required at lower excitation energies. This would most conveniently be performed in normal kinematics using a ^{10}Be target and a ^{4}He beam.

[1] M. Itoh *et al.*, Nucl. Phys. A **738**, 268 (2004).
[2] M. Itoh *et al.*, Phys. Rev. C **84**, 054308 (2011).
[3] M. Freer *et al.*, Phys. Rev. C **80**, 041303(R) (2009).
[4] W. R. Zimmerman, N. E. Destefano, M. Freer, M. Gai, and F. D. Smit, Phys. Rev. C **84**, 027304 (2011).
[5] W. R. Zimmerman *et al.*, Phys. Rev. Lett. **110**, 152502 (2013).
[6] M. Freer *et al.*, Phys. Rev. C **83**, 034314 (2011).
[7] D. J. Marín-Lámbarri, R. Bijker, M. Freer, M. Gai, T. Kokalova, D. J. Parker, and C. Wheldon, Phys. Rev. Lett. **113**, 012502 (2014).
[8] T. Suhara and Y. Kanada-En'yo, Phys. Rev. C **82**, 044301 (2010).
[9] M. Milin and W. von Oertzen, Eur. Phys. J. A **14**, 295 (2002).
[10] W. von Oertzen *et al.*, Eur. Phys. J. A **21**, 193 (2004).
[11] N. Soić *et al.*, Phys. Rev. C **68**, 014321 (2003).
[12] D. Price *et al.*, Phys. Rev. C **75**, 014305 (2007).
[13] D. Price *et al.*, Nucl. Phys. A **765**, 263 (2006).
[14] P. Haigh *et al.*, Phys. Rev. C **78**, 014319 (2008).
[15] M. Milin *et al.*, Nucl. Phys. A **730**, 285 (2004).
[16] K. P. Artemov *et al.*, Sov. J. Nucl. Phys. **52**, 406 (1990).
[17] Micron Semiconductor Ltd., 1 Royal Buildings, Marlborough Road, Churchill Industrial Estate, Lancing, Sussex, BN15 8UN, UK.
[18] T. Davinson, *et al.*, Nucl. Instrum. Methods A **454**, 350 (2000).
[19] R. E. Azuma *et al.*, Phys. Rev. C **81**, 045805 (2010).
[20] J. C. Pei and F. R. Xu, Phys. Lett. B **650**, 224 (2007).
[21] N. Itagaki, S. Okabe, K. Ikeda, and I. Tanihata, Phys. Rev. C **64**, 014301 (2001).
[22] N. Itagaki, T. Otsuka, K. Ikeda, and S. Okabe, Phys. Rev. Lett. **92**, 142501 (2004).
[23] T. Suhara and Y. Kanada-Enyo, Phys. Rev. C **84**, 024328 (2011).